Hydrogeology Journal (2025) 33:2003–2021
https://doi.org/10.1007/s10040-025-02953-9

REPORT

Hydrochemistry, stable isotopes, and radon in waters of the Greater Timbavati catchment, South Africa

Kirsten Raible[1] · **Roger E. Diamond**[2] · **Matthys A. Dippenaar**[1]

Received: 23 July 2024 / Accepted: 29 August 2025 / Published online: 30 October 2025

Abstract

A baseline study was conducted to better understand the relationship between groundwater, geology, and geography in the Greater Timbavati area, South Africa. Samples of rainwater, surface water, and groundwater were collected across nature reserves and rural communities. Basic water chemistry parameters, nitrates, and ammonium were measured in the field using an Aquaread AP-5000 probe, and water samples were collected for radon determination and stable isotope analysis. Significant differences in chemistry and isotopic signatures between surface water and groundwater were observed. Groundwater exhibited a mean total dissolved solids (TDS) of 1217 mg/l and pH of 7.5, whereas surface water had mean TDS of 332 mg/l and pH of 8.3. Groundwater δ^2H and $\delta^{18}O$ means were – 20.5 and – 3.8‰, respectively, contrasting with + 12.2 and + 2.3‰ in surface water. Hydrochemistry correlated with bedrock type and a close correlation between land use and nitrate concentrations was evident, particularly in groundwater, exceeding 500 mg/l in areas with dense human and livestock presence, suggesting urban and agricultural contamination. Radon concentrations in groundwater ranged from 188 to 51,400 Bq/m^3, showing no clear correlation with underlying geology, suggesting groundwater flow paths across bedrock types. Overall, a strong distinction between groundwater and surface water characteristics suggests limited interaction, caused by deep water tables, especially at the end of the dry season when streams stop flowing, warranting further research in quantifying sustainable levels of groundwater abstraction.

Keywords Nitrates · Radon · Environmental tracers · Hydrogeology · South Africa

Introduction

The importance of groundwater in the Greater Timbavati area

Groundwater is a critical resource in the Greater Timbavati area, South Africa, providing water to both rural communities and nature reserves. As the primary source of water in this semi-arid region, understanding the complex relationships between hydrogeology, surface water, and groundwater is essential for sustainable management. However, increasing pressures from land use changes, agriculture, and population growth have created a growing need to assess the hydrochemical and isotopic properties of these water resources. This study aims to address this knowledge gap by establishing a baseline understanding of the hydrochemistry and isotopic signatures of groundwater and surface water in the Greater Timbavati catchment. By examining the interactions between groundwater and surface water and exploring the effects of geology and human activity on water quality, this research contributes towards broader efforts to safeguard water resources in this environmentally sensitive region.

Objectives

To achieve this aim, the study pursued the following specific objectives: (1) Analyze the chemical composition of groundwater and surface water samples across the Greater Timbavati area; (2) Assess the spatial variation in key water quality parameters (pH, total dissolved solids, nitrates, ammonium)

This article is part of the topical collection "Progress in groundwater investigation, monitoring and management in South Africa".

✉ Kirsten Raible
kirstenraible@gmail.com

[1] Department of Geology, University of Pretoria, Pretoria, South Africa

[2] BIOGRIP, Department of Geological Sciences, University of Cape Town, Cape Town, South Africa

in relation to different land use types and underlying geological formations (3) Investigate the isotopic signatures (δ^2H and $\delta^{18}O$) of groundwater and surface water to trace recharge sources and identify potential groundwater–surface water interactions; (4) Measure radon concentrations in groundwater and surface water, to explore their relationship with geological structures; and (4) Provide a baseline water quality assessment to inform future management and strategies for mitigating contamination.

Literature review

Hydrochemistry

The chemical composition of groundwater and surface water is influenced by multiple factors, including geology, land use, and climatic conditions. Key parameters such as pH, total dissolved solids (TDS), and major ions (e.g., sodium, potassium, calcium, chloride, and bicarbonate) provide insight into the geochemical processes that shape water quality.

Groundwater quality in hard rock aquifers, such as those in the Greater Timbavati area, is generally of higher quality than surface water, but it remains vulnerable to pollution from land use changes due to the shallow nature of these aquifers (Wright 1992; Lachassagne et al. 2021). The weathering of minerals in bedrock significantly contributes to the ion composition of groundwater, where variations in TDS often indicate water–rock interactions. High levels of TDS can be associated with the dissolution of minerals, whereas lower levels may indicate dilution with meteoric water.

Nitrate contamination is a particular concern in many parts of southern Africa due to its potential health risks and its role as an indicator of human impact on water resources. High nitrate concentrations in groundwater may occur naturally in specific climate and topographical conditions but are more commonly linked to human activities, such as agriculture and sanitation (Tredoux et al. 2009; Baloyi and Diamond 2019). In developed regions, agriculture is the main source of nitrate pollution, while in southern Africa, the main source is from on-site sanitation (Tredoux et al. 2009; Graham and Polizzotto 2013). Several studies have highlighted the risks posed by unlined pit latrines, which result in the leaching of nitrates and pathogens into shallow groundwater systems (McGill et al. 2019; Masindi and Foteinis 2021).

Beyond nitrate, other hydrochemical parameters, including ammonium, chloride, and bicarbonate, are important for understanding the water quality and its suitability for human consumption and ecological health. Dube et al. (2020) found that groundwater quality in Limpopo Province varied significantly across land use types, with the highest nitrate concentrations in areas of subsistence farming and lower in urbanized regions. Phungela et al. (2022) similarly noted that wastewater treatment effluent introduced multiple contaminants into surface water systems, including nitrates from residential and agricultural waste. Baloyi and Diamond (2019) also found large variations in water quality in a small suburban area north of Pretoria, including some dangerously high levels of nitrate, fluoride, and pathogenic bacteria, concluding that differences in pollution sources, natural and anthropogenic, and vadose zone processes might account for the observed water quality variations.

Stable isotopes

The isotopic composition of groundwater can provide information relating to recharge sources, transport mechanisms, and the interaction between different water bodies (Yeh and Lee 2018). Different isotopes of the same element behave differently under the same physical, chemical, and biological processes due to differences in their masses, resulting in fractionation. Due to isotopic fractionation, meteoric water in different regions has different compositions of stable hydrogen and oxygen isotopes. When meteoric water seeps into aquifers, its isotopic signature allows groundwater to be traced along flow pathways and used as a basis for detecting recharge sources. Many hydrogeological studies (e.g., Abiye et al. 2021; Diamond and Harris 2019; Ding et al. 2013; Hao et al. 2019; Harkness et al. 2018; Peng et al. 2016; Petersen et al. 2023; Yeh and Lee 2018 and Zhu et al. 2019) use stable hydrogen and oxygen isotopes of water as natural tracers for identifying recharge sources, as unlike artificial tracers, they are naturally occurring in the groundwater.

Stable isotope concentrations are normally presented as the ratio of the least abundant isotope over the most abundant isotope and expressed relative to a standard. This is known as δ notation and expresses the deviation of the isotopic ratio (R) of the sample from the standards as seen in Eq. 1. The internationally agreed standard for water is Standard Mean Ocean Water (SMOW), with the isotopes present in the ratios $^{18}O/^{16}O = 2.005 \times 10^{-3}$ and $^{2}H/^{1}H = 1.56 \times 10^{-4}$ (Appelo and Postma 2005).

$$\delta_{\text{sample}} = \frac{R_{\text{sample}} - R_{\text{standard}}}{R_{\text{standard}}} \times 1000 \quad (1)$$

where

$$R = \frac{^{18}O}{^{16}O} \text{ or } \frac{^{2}H}{^{1}H}$$

Craig (1961) was the first to demonstrate a specific relationship between hydrogen and oxygen isotope distribution in atmospheric precipitation due to continuous fractionation caused by evaporation and precipitation processes, and analyzed the global $\delta^{18}O$ and δD isotope compositions of

rain, snow, and river water samples, using linear regression to obtain the Global Meteoric Water Line (GMWL), with an equation of $\delta D = 8 \times \delta^{18}O + 10$ ‰. Local meteoric water lines (LMWLs) are simplified representations of average $\delta^{18}O$ and δD relationships at a site and are often evaluated based on their deviation from the GMWL. LMWLs can be used to provide a reference framework for interpreting isotope ratios measured in terrestrial waters (Putman et al. 2019).

Radon

Uranium and radium are the radioactive precursors of radon and are present in virtually all types of rocks and soil, with the amount of these elements varying from site to site and different geological materials (Tommasino 2005). During the radioactive decay of radium, a radon atom and its alpha particle sibling recoil from one another upon their formation; this is a violent process that propels them in opposite directions and can result in their liberation from the surrounding rock (Baskaran 2016). The concentration of radon in groundwater depends largely on the mineralogy and structure of the surrounding rock (Litt et al. 1992). Studies in the New Jersey Highlands, USA, and Sweden reveal that granitic, pegmatitic, and felsic volcanic rocks, as well as fractured gneisses, are more likely to yield elevated radon levels due to their high uranium content and structural porosity (Litt et al. 1992; Knutsson and Olofsson 2002). In a study of the Table Mountain Group aquifer in South Africa, conducted by Strydom et al. (2021), high groundwater radon concentrations were associated with uranium-rich granite and extensive fracturing. Similarly, research in Ethiopia's Upper Awash Basin showed that fractured basaltic and ignimbrite formations can yield high radon values in groundwater, demonstrating how geological formations influence radon levels (Tadesse et al. 2023).

Statistical analyses conducted by Cho and Choo (2019) on the geochemical behavior of uranium and radon in groundwater revealed no close correlations between uranium and radon. Radon, unlike uranium, appeared to migrate independently with respect to most geochemical parameters. However, Cho et al. (2015) noted that radon concentrations correlated with hydrogeological components such as oxidation-redox potential (Eh), electrical conductivity (EC), and sample depth.

A study in Sweden conducted by Knutsson and Olofsson (2002) noted a positive correlation between high groundwater radon concentrations in drilled wells for granites, pegmatites, felsic volcanics and some felsic gneisses. Alabdula'aly (2014) and Cho et al. (2015) found that the radon levels in shallow aquifers were generally higher than those in deep aquifers, as dissolved radon tends to move upwards along fractures due to the decrease in hydrostatic pressure. On the other hand, Cho et al. (2019) found that average groundwater radon concentrations were higher when sampling deeper wells in South Korea compared to earlier studies that sampled shallower wells, such as Cho et al. (2007). Cho et al. (2019) believed that this was due to radon in the shallow aquifers being able to escape more easily than radon in deep aquifers.

Radon present in surface water is mostly derived from the inflow of radon-rich groundwater, but it is quickly lost to the atmosphere via outgassing (Grolander 2009). Its concentration can fluctuate with seasonal cycles, as observed in South Korea. There, radon concentrations in a riverside groundwater system varied according to changes in river flow and groundwater inflows, illustrating the utility of radon as a tracer in dynamic groundwater–surface water systems (Kim et al. 2020). Despite these influences, studies show that radon often migrates independently of uranium or other geochemical parameters (Cho and Choo 2019), suggesting its concentration is more influenced by hydrodynamic factors than solely by rock type.

Study area

Location

The Greater Timbavati catchment is located within the Lowveld region of South Africa in both the Mpumalanga and Limpopo provinces near the Kruger National Park. In South Africa, hydrological catchments are subdivided and denoted by alphanumeric codes (e.g., B73E), with the study area specifically including the B73E and X40C subdivisions (DWS 2017). According to the 'Olifants Water Management Area: Internal Strategic Perspective' compiled by the Department of Water Affairs and Forestry (DWAF 2004), the area is characterized by having large agricultural developments, including irrigation and large game management areas, including the western portion of the Kruger National Park.

Climate

The lowveld climate is known for having a hot and humid summer with a mild and dry winter. The climate of southern Africa is influenced by anticyclonic systems that cyclically move from east to west (Venter and Gertenbach 1986). Based on the Köppen climate classification system, the study area has a Cwa subtropical climate. The mean annual precipitation in the catchment is generally less than 500 mm but can reach up to 1000 mm toward the western boundary near the southern African escarpment.

Geology

The geology of the study area is presented in Fig. 1. The Makhutswi Gneiss outcrops in the north and south of the study area. The Makhutswi Gneiss is light grey, fine to medium-grained with alternating leucosome bands of up to 15 cm and complexly folded (Schutte 1986; Walraven 1989; Robb et al. 2006). The major minerals found in the rock are plagioclase, microcline, quartz and biotite, with hornblende and pyroxene occurring infrequently. Limited geochemical data from the area suggest that the Makhutswi Gneiss is tonalitic to granodioritic in composition. Remnants of ultramafic, amphibolite, metaquartzite, and calc-silicate rocks are also found within the Makhutswi Gneiss (Schutte 1986; Robb et al. 2006). Poujol et al. (1996) attributed the age of the Makhutswi gneiss to be 3228 ± 12 Ma when sampling close to the contact with the Murchison Greenstone Belt; and Barton (1984) determined its age to be 3268 ± 113 Ma in the Phalaborwa area. A younger tonalitic, unmigmatized biotite gneiss is locally intruded as dyke or stock-like bodies and dated by Brandl and Kröner (1993) to be 3112 ± 5 to 3078 ± 6 Ma (Robb et al. 2006).

The Klaserie Gneiss is located between the two sections of Makhutswi Gneiss and is in contact with the Nelspruit Suite and Cunning Moor Tonalite. The Klaserie Gneiss has a very similar mineralogy to the Makhutswi Gneiss but is coarse-grained, well foliated, and non-migmatized (Walraven 1989; Robb et al. 2006). It is approximately situated at the boundary between the southern section of the Makhutswi Gneiss, the Nelspruit Suite, and the Cunning Moor Tonalite body. The Klaserie Gneiss is believed to post-date the Makhutswi Gneiss but there are no radiometric ages available (Robb et al. 2006). Around 1106–1112 Ma, large-scale magmatism resulted in the emplacement of huge volumes of mantle-derived magmas, over 2 million km^3, into the Palaeoarchaean to Mesoproterozoic formations and cratonic basement rocks of the Kaapvaal Craton. The group is known as the Umkondo Igneous Province and includes intrusions such as the Timbavati Gabbro (Allsopp et al. 1989; Hanson et al. 2004; Anhaeusser et al. 2006). The Timbavati Gabbro consists of mafic to ultramafic rocks that have intruded into various older granites, gneisses, and magmatic Archaean basement rocks of the Mpumalanga Lowveld. Discontinuous outcrops occur as a series of small hills and ridges, following a rough zig-zag pattern, in the western half of the Kruger National Park (Brandl 1985; Saggerson and Logan 1970; Walraven 1986, 1989; Walraven and Hartzer 1986; Anhaeusser et al. 2006). The intrusions appear sill-like in

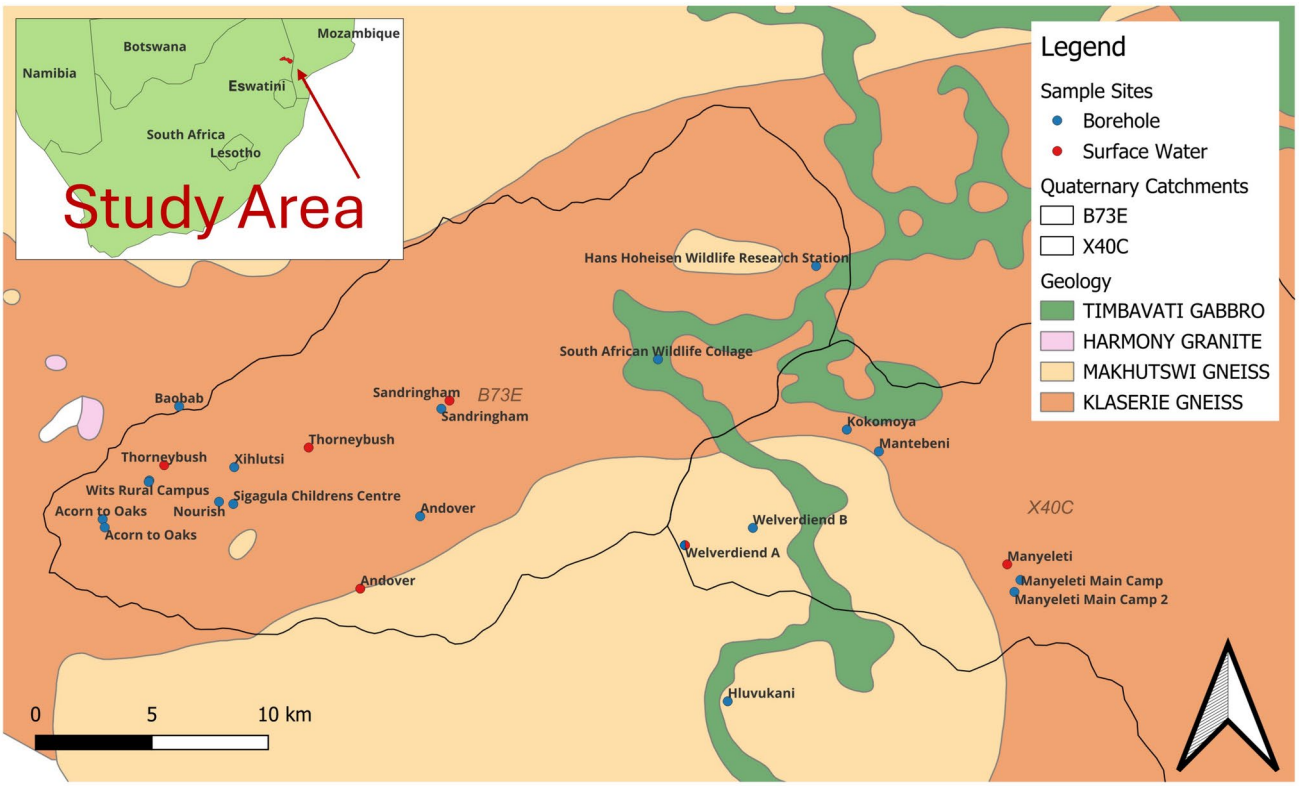

Fig. 1 Location of the study area, with the *B73E* and *X40C* catchment boundaries shown in *black*. Sample sites are marked in *red* for surface water and *blue* for groundwater, and labeled with their respective site names, all overlaid on the underlying geology (Council for Geoscience n.d.; Esri 2023)

nature and dip between 20 and 30 degrees towards the east (Schutte 1986). In the Orpen area, the sills are believed to be about 200 m wide (Gordon-Welsh 1980), whereas in the Pretoriuskop area, they range between 300 and 480 m wide (Clubley-Armstrong 1979). A chilled margin is present at the contact between the host rocks and the gabbro, with the host rock showing various degrees of recrystallisation (Schutte 1986). The Timbavati Gabbro consists primarily of olivine, clinopyroxene, orthopyroxene, and plagioclase (Walraven 1986).

Hydrogeology

According to the Olifants Water Management Area: Internal Strategic Perspective (DWAF 2004), the main use of groundwater in the area is for domestic use and stock watering. While groundwater quality is generally good, there are isolated areas with elevated nitrate concentrations. Aquifers are restricted to weathered and fractured bedrock zones and boreholes are between 30 and 80 m deep with water levels between 5 and 15 m below ground level (m b.g.l.). Boreholes generally yield between 0.5 and 2 l/s, but in areas east of Hoedspruit this can increase to 5 l/s. According to data obtained from Groundwater Resources of South Africa Map Series, 1995, groundwater recharge is between 25 and 37 mm/a in the westernmost section of the B73E quaternary catchment and decreases to 10–15 mm/a in the B73F quaternary catchment (DWAF 2004).

Methods

Sampling took place from September 2021 until November 2022. From the boreholes and surface water bodies identified in a hydrocensus, six surface water sample points and 19 groundwater sample points were chosen (Fig. 1). All sampling was done in accordance with the South African Bureau of Standards (SABS) ISO 5667 (2022) guidelines. Five rounds of sampling were conducted to obtain data that reflected seasonal variations in the water chemistry. A total of 100 samples could have been collected; however, due to unforeseen circumstances, some samples could not be collected. Rainwater samples were collected and rainfall totals (mm) were recorded at two sites, Hans Hoheisen Wildlife Research Station and Manyeleti Main Camp for isotope analysis.

Rainwater was collected in a rain gauge and rainfall volumes were recorded every morning at 08:00, corresponding to the previous day's precipitation. Rainwater was then poured into a 5-l bottle, and the lid was tightly sealed to prevent evaporation. At the end of the month, the 5-l bottle was shaken to ensure the water was well mixed, including the water droplets on the side of the bottles. The water was then poured into two smaller 50-ml bottles, to the top if possible, and the lid tightly sealed to prevent evaporation. The bottle was then labeled with the respective month and location.

Equipment was cleaned, checked and, if necessary, calibrated daily. During sampling, the equipment was rinsed in sample water. Samples were collected in two PET sample bottles (for isotope analysis) and the Aquaread AP-5000 calibration cups. As all the boreholes being sampled were equipped with pumps, taps or pipes were opened to allow access to the borehole water as close to the pump as possible and before water entered a storage tank. Water was collected from the larger surface water bodies using a bailer before being transferred to sample bottles and into the calibration cup. Sample bottles were then sealed and labeled with the sample name and date of sampling; no preservation techniques were used.

The Aquaread AP-5000 was used in the field to measure the following parameters: temperature, pH, dissolved oxygen (DO), electric conductivity (EC), total dissolved solids (TDS), salinity (SAL), oxidation–reduction potential (ORP), nitrate (NO_3^-), and ammonium (NH_4^+). The Aquaread AP-5000 required daily single-point calibration using a known concentration solution, e.g., 10 ppm, and a weekly two-point calibration, e.g., with 10 and 100 ppm solutions, to maintain measurement accuracy across the various parameters. The Aquaread AP-5000 was inserted into the calibration cup for analysis instead of lowering the probe into the boreholes because of well instrumentation. The equipment was then cleaned and dried before being stored. In the Aquaread manual (2021) the optical electrodes are described as being standalone, fixed-frequency fluorometers specifically tuned to excite and detect the fluorescence of selected substances in water. This is achieved by emitting short pulses of high-energy light at the excitation wavelength and responding to fluorescence in the detection range. Inaccuracies in measurements can be due to microbiological species, compounds that fluoresce at similar wavelengths, and differences in fluorescence caused by temperature, ambient light, and turbidity.

The Durridge RAD7 was used for the radon analysis. The device works by using an electrostatic collection of alpha emitters with a spectral analysis. The passivated ion-implanted planar silicon detector SNIFF mode counts polonium-218 decays while the normal mode counts both polonium-218 and polonium-214 decays (Durridge Company Inc 2022). Samples were taken back to camp and analyzed there, as it was not possible to take the RAD7 instrument into the field. Samples were analyzed as soon after sampling as possible, usually within 12 h and often within 6 to 8 h. Before the samples were analyzed, the machine was purged for 10 min with the system open to atmosphere but still being connected to the drying unit. This was done to remove any excess radon from the system left behind by previous

analyses. After 10 min, the system was closed to recycle air, and the purging continued until the relative humidity reading had dropped below 6%. The sample was analyzed, and the results were printed afterwards. The same purging and drying process was completed between every sample analysis to prevent cross-contamination. Another precaution taken to prevent cross-contamination was to run the samples in order of least presumed radon to most presumed radon, i.e., surface water samples were analyzed before groundwater.

Rainwater, groundwater, and surface water samples were taken to iThemba LABS in Johannesburg, where hydrogen and oxygen isotope ratios were analyzed in the Environmental Isotope Laboratory (EIL). The analysis was done using a Los Gatos Research (LGR) liquid water isotope analyzer, and laboratory standards, calibrated against Standard Mean Ocean Water (SMOW), were analyzed with each batch of samples.

During the fourth round of sampling, both groundwater and surface water samples were collected for more detailed chemical analysis at the laboratory. Samples were collected in 500-ml PET bottles, sealed and labeled. The bottles were then placed in a cooler box and refrigerated until they could be delivered to Aquatico laboratory.

Results

General water quality

The pH values of the groundwater samples range from 6.97 to 8.40 with a mean value of 7.48; and the pH values of the surface water samples range from 7.47 to 9.3 with a mean value of 8.30. Groundwater TDS values ranged from 540 to 3580 mg/l with a mean value of 1220 mg/l. Surface water samples ranged from 140 to 620 mg/l with a mean value of 330 mg/l. While there appears to be a trend of decreasing TDS with increasing pH as shown in Fig. 2, Pearson's r values show no correlation with – 0.15 for the groundwater samples and a minimal correlation of – 0.5 for the surface water samples. The ORP values of the groundwater samples range from 19 to 200 mV with a mean of 99 mV, while those of the surface water samples range from 35 to 196 mV with an average of 91 mV. Pearson's r values of 0.45 for the surface water samples show a minimal correlation between ORP and pH, while the groundwater samples show no correlation with $r = 0.20$ as shown in Fig. 2. DO concentrations of the groundwater samples range from 2.65 to 8.60 mg/l with a mean of 5.33 mg/l and surface water samples ranged from 6.26 to 12.66 mg/l with a mean of 8.22 mg/l. DO and pH have no correlation with Pearson's r values of 0.06 and 0.13 for the groundwater and surface water samples, respectively, as shown in Fig. 2.

NH_4^+ concentrations range from 0.01 to 0.75 mg/l with a mean value of 0.20 mg/l for the groundwater samples and 0.02 to 1.7 mg/l with a mean value of 0.34 mg/l for the surface water samples. There is minimal correlation between NH_4^+ and TDS in groundwater with a Pearson's r value of 0.47, however, there is no correlation in the surface water samples with an r value of 0.19 (Fig. 3).

NO_3^- groundwater concentrations range from 0.28 to 1350 mg/l with a mean value of 83.1 mg/l and surface water concentrations ranged from 1.59 to 10.4 mg/l with a mean value of 5.56 mg/l. The surface water samples show no correlation between nitrate and TDS with a Pearson's r value of – 0.19 but the groundwater samples show a better correlation ($r = 0.59$; Fig. 3).

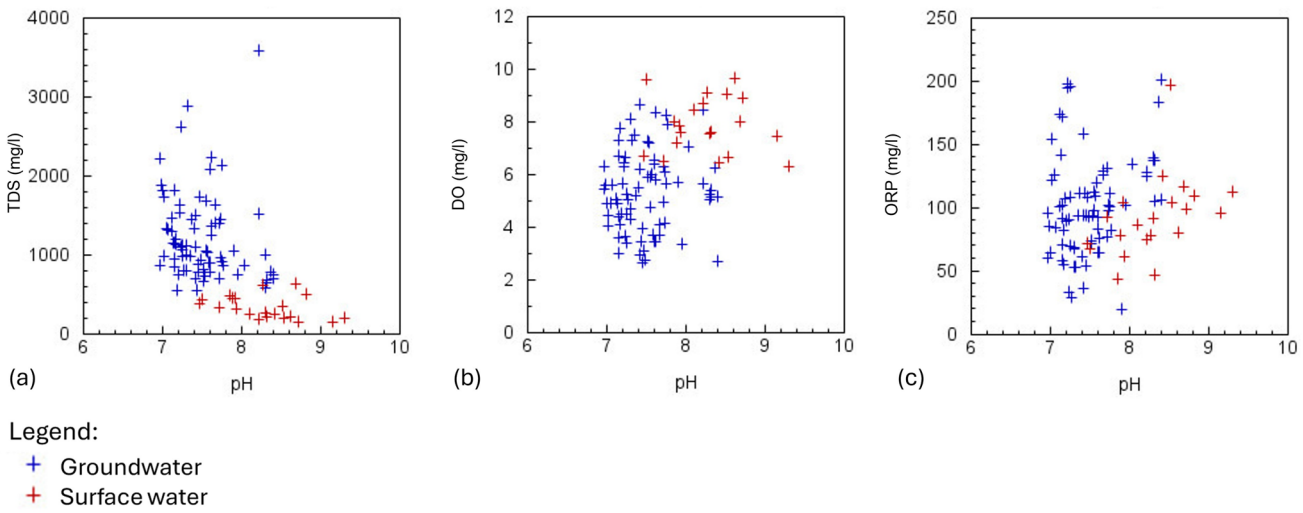

Fig. 2 Relationships between pH and: **a** TDS; **b** DO; and **c** ORP, for the five rounds of sampling

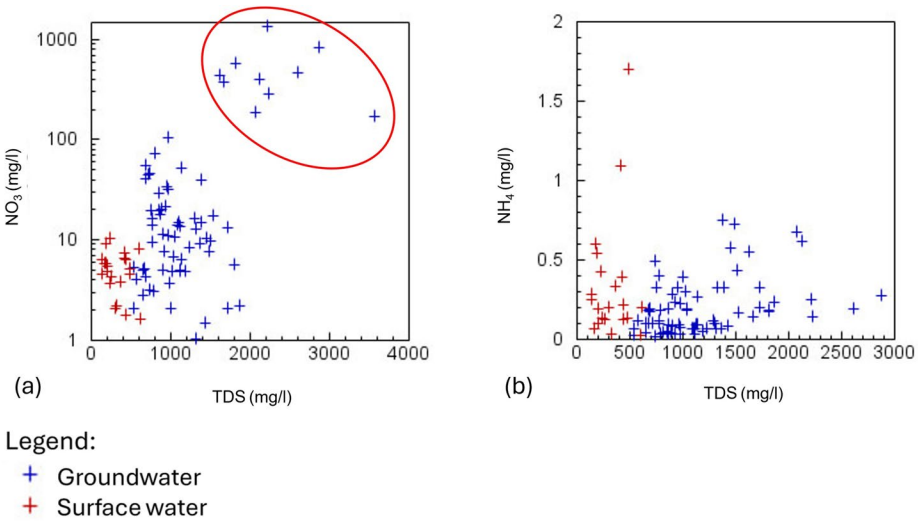

Fig. 3 Relationships between TDS and: **a** NO_3; and **b** NH_4 for all five rounds of sampling. *Circled in red* are the values for the samples taken at Welverdiend A, Welverdiend B, and Hluvukani which appear to be outliers

Figure 4 shows the comparison between the nitrate (NO_3^--N mg/l) concentrations measured with the Aquaread probe and those determined by Aquatico laboratory in Centurion. The Aquaread readings were two times higher than the laboratory measurements. When plotting the Aquatico concentrations against the Aquaread concentrations a near-perfect linear relationship can be observed, with a Pearson's *r* value of 0.9983. As the probe was verified and if necessary calibrated daily the cause of this difference was not sensor drift. The Aquaread AP-5000 probe has an accuracy of ~ 10% or 2 ppm of the reading (whichever is greater) but chloride, bromide, fluoride, sulphate, chlorate, and perchlorate ions could have interfered with the ISE electrode readings. When looking at the chemical data from the laboratory, it could be noted that WelA, HLU, and BAO had the highest chloride concentrations of 42.8, 98.3, and 81.4 mg/l, respectively, while WelA and HLU also had the highest sulphate concentration of 42.8 and 98.3 mg/l, respectively. However, the difference between the laboratory results and the Aquaread readings is consistent for all the samples, suggesting this is not the cause of the discrepancy. It is likely that the discrepancy in the concentrations is due to the difference in how long it took for the samples to be analyzed. The Aquaread analysis was done on-site while the laboratory was only able to analyze the samples a month after sampling took place, due to complications with the laboratory. Degassing of the samples likely took place during this time.

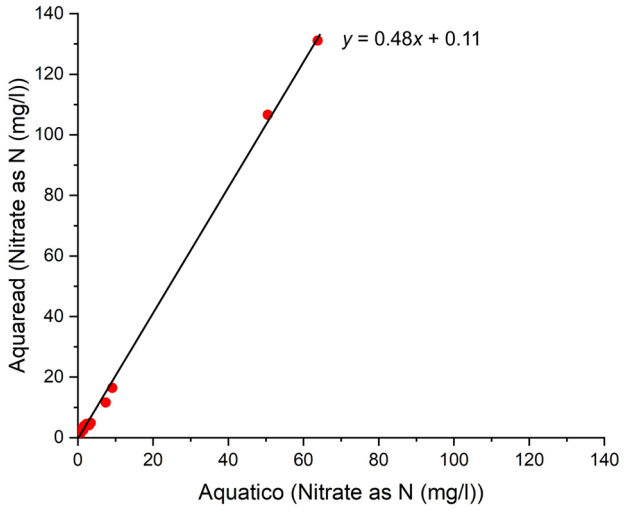

Fig. 4 Relationship between laboratory results and Aquaread NO_3 concentrations

From the Piper (Fig. 5) and Stiff plots (Figs. 6, 7, 8, and 9), it was observed that all but three of the water samples (WelA, HLU, and UPCell), featured similar cation and anion compositions. Most samples are located within the mixed cation and anion facies (Fig. 5). UPCell differed from the rest in that it falls into the magnesium bicarbonate type category. WelA and HLU are chloride types. When looking at the Schoeller diagrams (Figs. 10 and 11), it can be seen that, once again, all the groundwater samples but WelA, HLU, and UPCell followed the same trend. It appears that the surface water samples follow a similar trend to the groundwater samples but with less variation in the ion concentrations, except for THORSW1 which has a lower K^+ concentration more akin to those of the groundwater samples.

Isotopes

The δD for groundwater ranged from – 27.7 to – 0.8 ‰, and $\delta^{18}O$ values ranged from – 5.0 to 1.3 ‰ with mean values of – 20.5 and – 3.8 ‰, respectively. Surface water δD values ranged from – 14.2 to + 41.9 ‰, and $\delta^{18}O$ values ranged from – 2.2 to + 7.5 ‰ with mean values of + 12.2

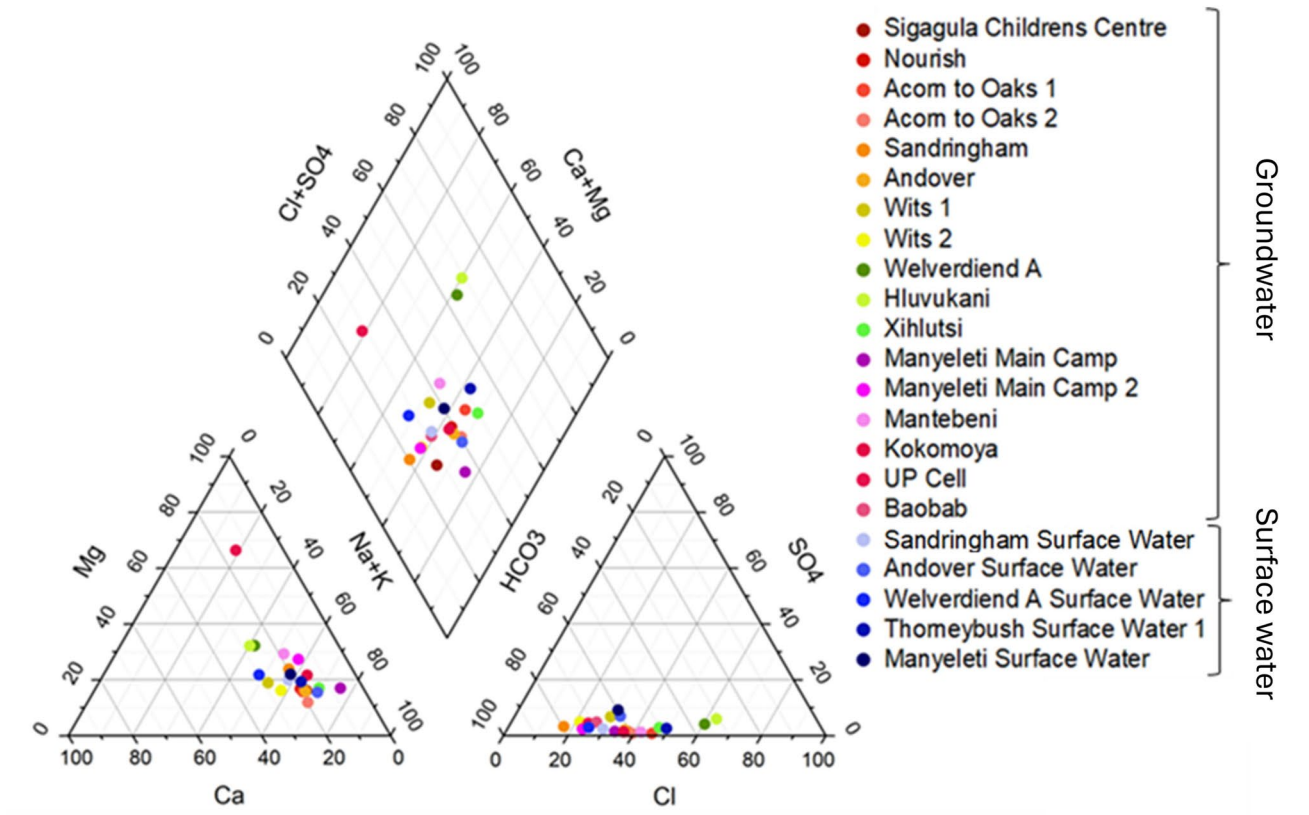

Fig. 5 Piper plot showing the chemistry of the ground and surface water samples collected during August and September 2022

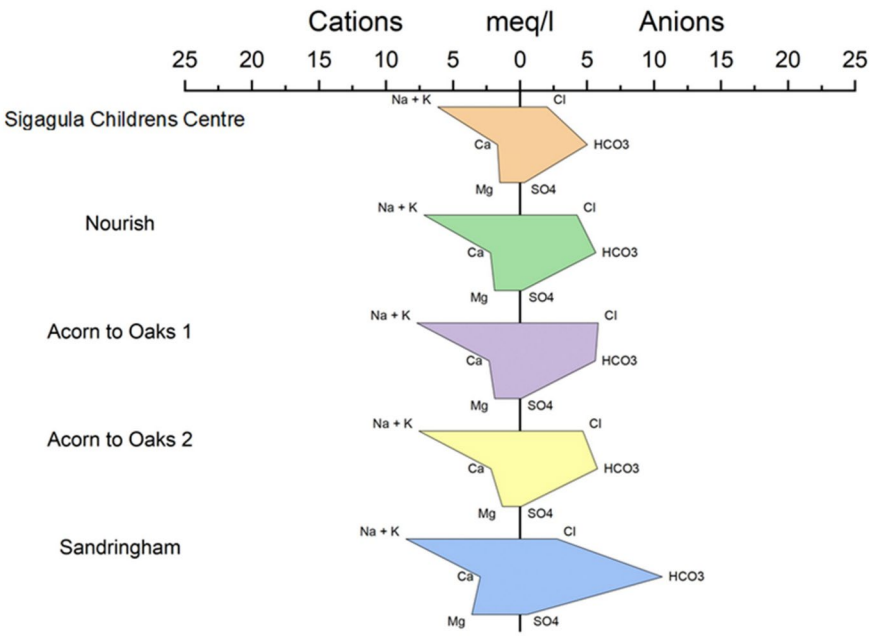

Fig. 6 Stiff plot showing the chemistry of the groundwater samples collected during August and September 2022

and + 1.3 ‰, respectively. The rainwater sample δD values ranged from – 24.9 to + 33.1 ‰, and $\delta^{18}O$ values ranged from – 4.8 to + 5.4 ‰ with weighted mean values of – 2.76 and – 1.9 ‰, respectively (Figs. 12 and 13). The surface water samples are enriched in heavier isotopes compared to the groundwater samples. There appears to be a seasonal variation in the surface water samples. δD and $\delta^{18}O$ values continued to increase as the dry season progressed, with the

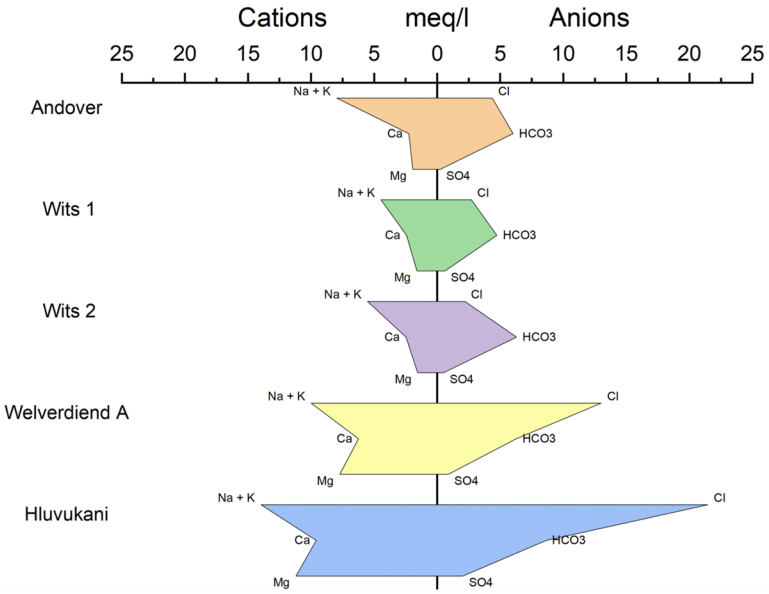

Fig. 7 Stiff plot showing the chemistry of the groundwater samples collected during August and September 2022

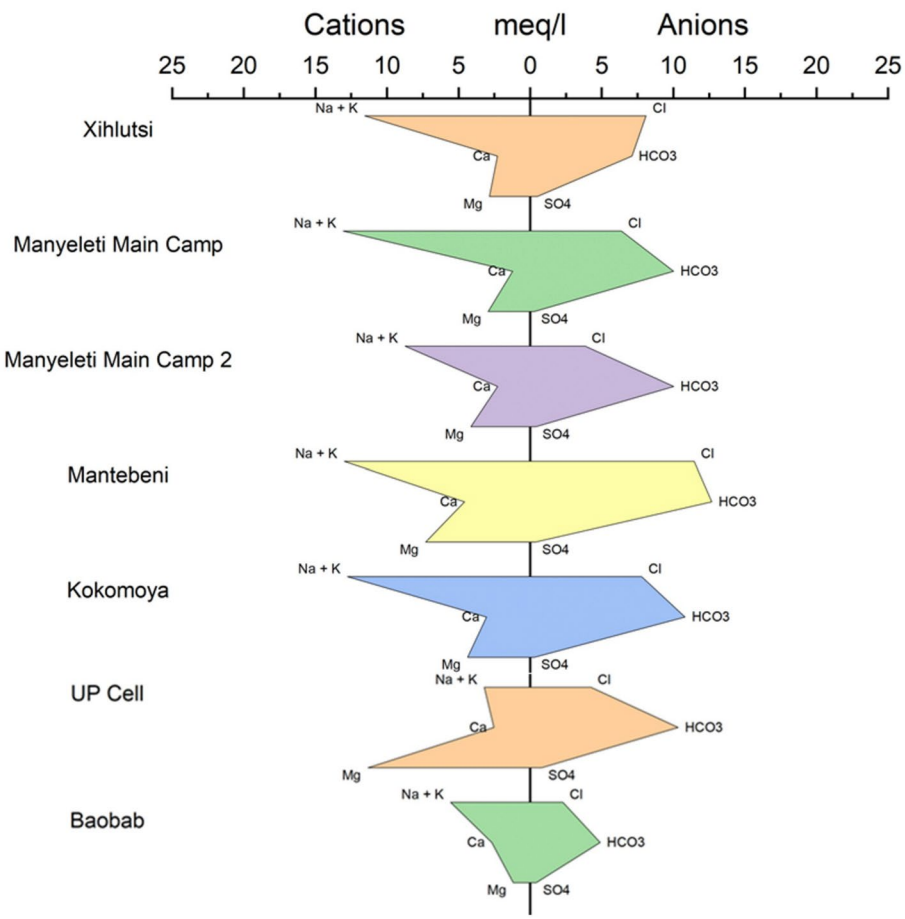

Fig. 8 Stiff plot showing the chemistry of the groundwater samples collected during August and September 2022

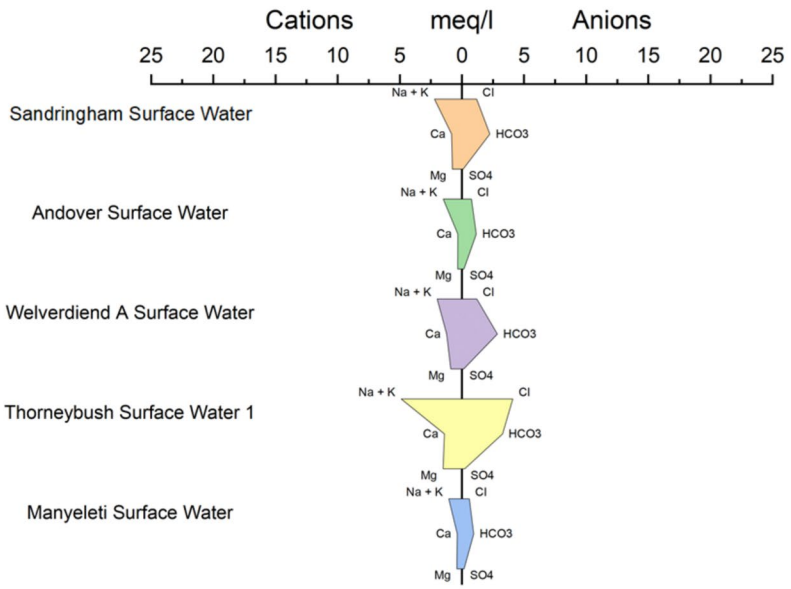

Fig. 9 Stiff plot showing the chemistry of the surface water samples collected during August and September 2022

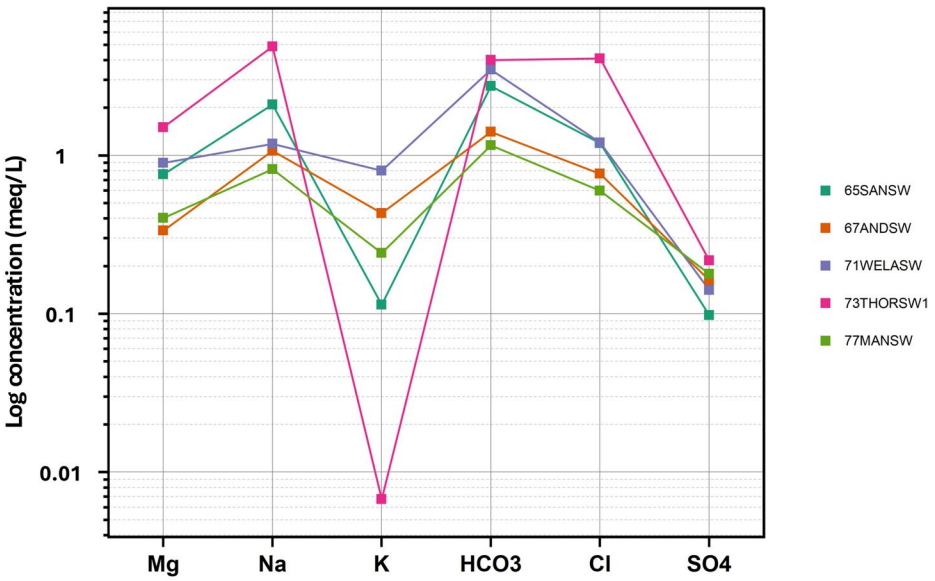

Fig. 10 Schoeller diagram showing the chemistry of surface water samples taken during August and September 2022

heaviest isotopic compositions occurring towards the end of the dry season (Figs. 12 and 14).

Radon

The RAD7 gives the arithmetic mean of the radon concentrations of four 5-min measurements per sample and the highest and lowest radon concentrations, as well as the standard deviation of the readings taken during the analysis. The mean surface water radon concentrations ranged from 0 to 522 Bq/m^3 and had an average concentration of 119 Bq/m^3 while the mean groundwater sample concentrations ranged from 188 to 51,400 Bq/m^3 with an average of 16,900 Bq/m^3 (Fig. 15).

Discussion

This study has provided a comprehensive analysis of groundwater and surface water chemistry in the Greater Timbavati area. The chemical composition and isotopic signatures of the water samples reveal important trends in relation to local geology, land use, and potential contamination sources.

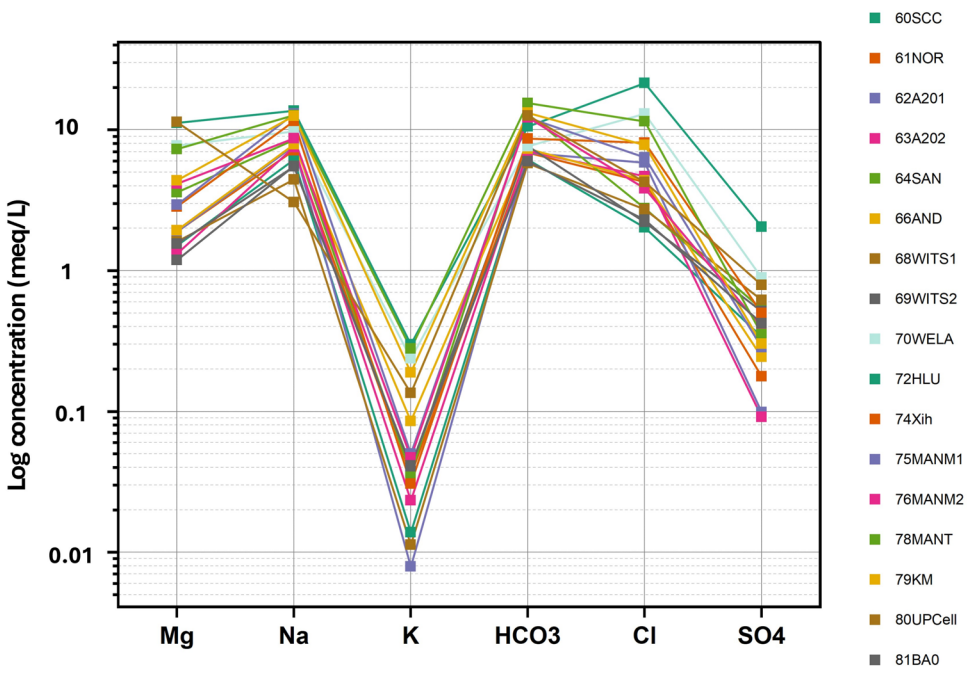

Fig. 11 Schoeller diagram showing the chemistry of groundwater samples taken during August and September 2022

From Fig. 2 it is evident that the relationships between TDS, ORP, DO, and pH for the groundwater and surface water samples cluster separately. Groundwater and surface water TDS values are compared to the $\delta^{18}O$ compositions of the samples in Fig. 16. Higher TDS values are found in the groundwater samples; however, these samples also have the lowest $\delta^{18}O$ values. During evaporation, the isotopically lighter water molecules (e.g., $^{1}H^{1}H^{16}O$) evaporate first, leaving behind liquid water that is enriched in heavier isotopes (e.g., $^{1}H^{2}H^{16}O$ and $^{1}H^{1}H^{18}O$). The lighter isotopic composition of groundwater suggests that little to no evaporation has taken place. The heavier isotopic composition found in the surface water samples is evidence of evaporation. Since the TDS values in the surface water samples are significantly lower than those of the groundwater samples, this is evidence that the source of the solutes is from weathering and water–rock interactions and not from evaporation.

The sample sites overlying the corresponding geology can be seen in Fig. 1. Based on the cation and anion concentrations of the groundwater samples, as observed in the Piper plot, Schoeller diagrams, and Stiff plots, the samples can be divided into three groups.

Most of the samples fall into group 1. They have a composition where $Na^+ + K^+$ is the highest cation concentration and HCO_3^- is the highest anion concentration. The samples that belong to this group are SCC, NOR, A201, A202, SAN, AND, Xih, MANT, KM, WITS1, WITS2, BA0, MANM1, and MANM2. All group 1 sample sites are located on the Klaserie Gneiss.

Group 2 samples were primarily located on the Makhutswi Gneiss. They have a composition where Na^+ and K^+ are the dominant cations and Cl^- is the dominant anion. The samples that belong to this group are WELA and HLU. The average groundwater HCO_3^-concentration of WELA and HLU is very close to the average of group 1, 455 and 459 mg/l, respectively. However, the average chloride concentrations are significantly higher, averaging 611 mg/l in WELA and HLU compared to the average of 174 mg/l in group 1. According to Hunt et al. (2012), high Cl^- levels can be regarded as an indicator of marine influence, evaporation, or pollution.

UPCell is the only sample in group 3. It has a composition where Mg^{2+} is the most abundant cation and HCO_3^- is most abundant anion concentration. While the geological map shows UPCell to be situated on the Klaserie Gneiss, the presence of Timbavati Gabbro outcrops in the vicinity of the sampling site suggests that the map is incorrect in this area.

Surface water samples featured much lower TDS values than the groundwater samples. All of the surface water samples, with the exception of THORSW1, have the same ion composition as group 1, whereas THORSW1 has the same composition as the samples in group 2 but is not located on the Makhutswi Gneiss.

The high Na^+ concentrations in the groundwater samples of groups 1 and 2 are most likely derived from the weathering of albite. Whereas K^+ is likely derived from the weathering of microcline and biotite and Ca^{2+} ions in the water samples are likely derived from the weathering of anorthite. The high Mg^{2+} concentrations in the UPCell sample are likely from the weathering of pyroxene and possibly olivine, while Ca^{2+} and Na^+ ions are from the weathering of plagioclase. The high HCO_3^- concentrations in the groundwater samples

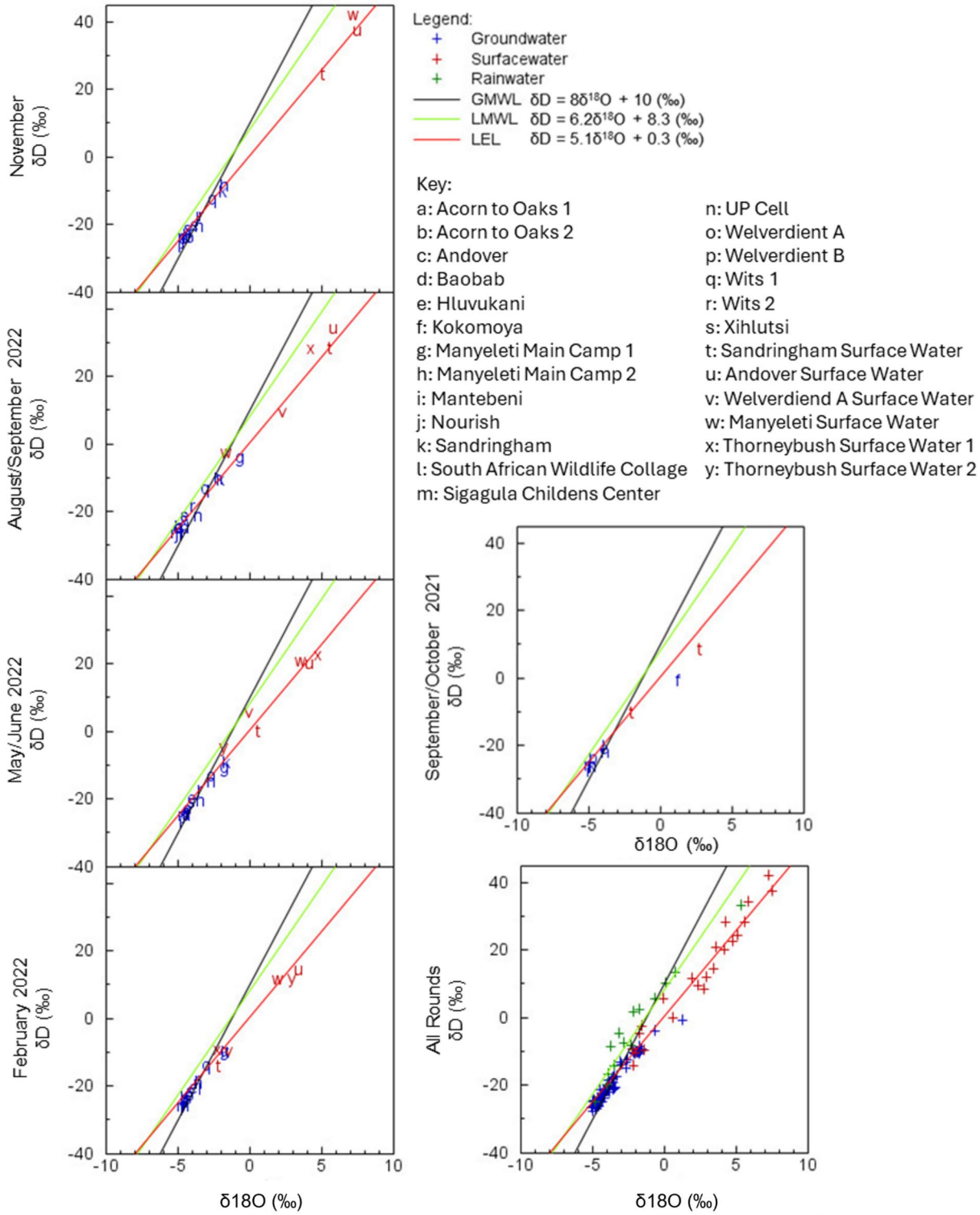

Fig. 12 $\delta^{18}O$ vs. δD for all five rounds of sampling

are a by-product of the silicate weathering process. Al^{3+} is likely derived from the weathering of microcline and biotite while Mg^{2+} and Fe are also from biotite.

NO_3^- concentrations were higher in the groundwater samples than in the surface water samples. It was evident that the NO_3^- concentrations from Welverdiend A,

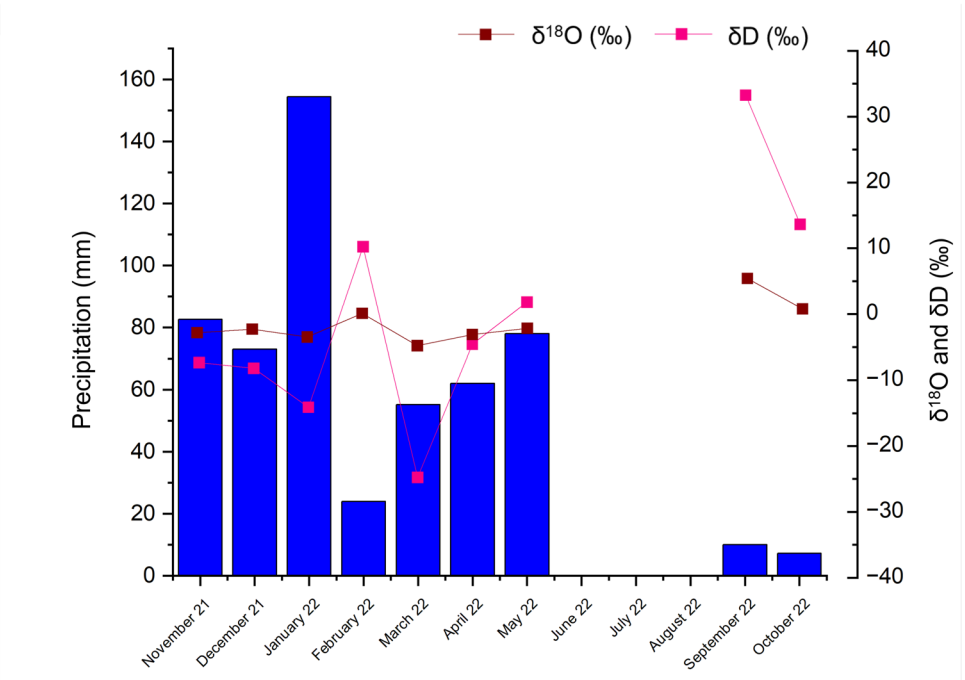

Fig. 13 Monthly precipitation at Hans Hoeheisen and corresponding hydrogen and oxygen isotope compositions

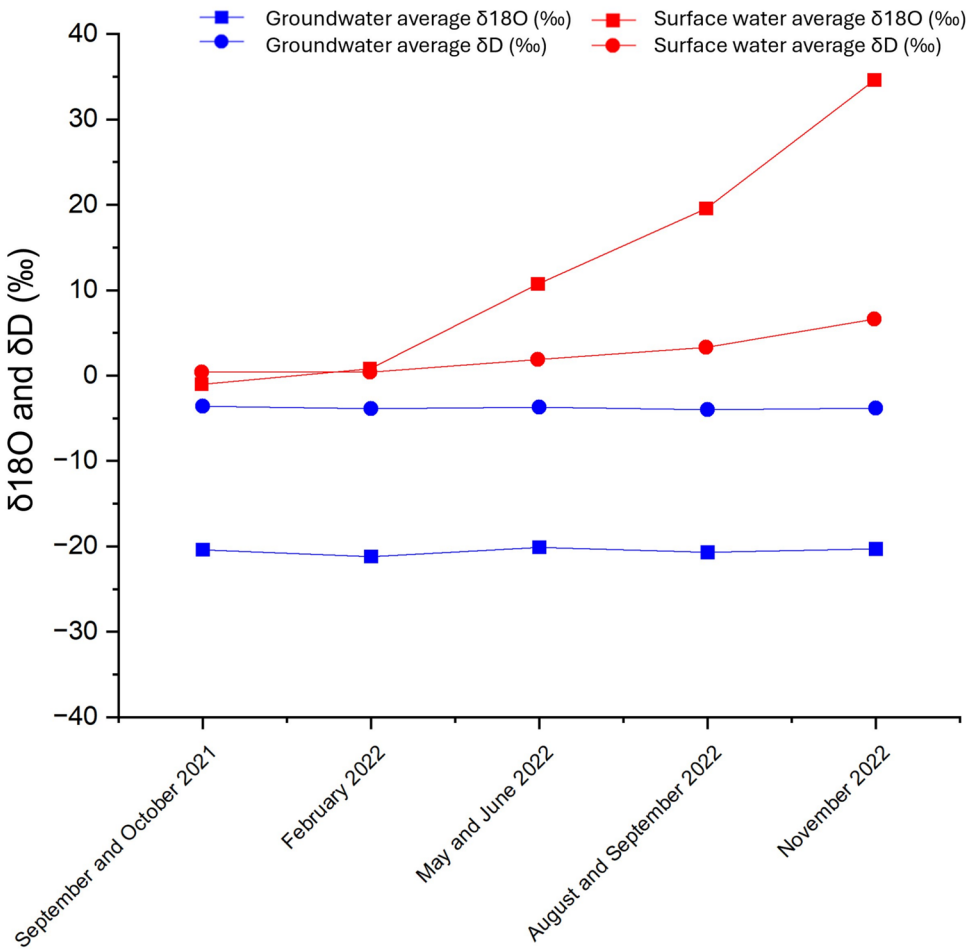

Fig. 14 Average δD (‰) and $\delta^{18}O$ (‰) for the groundwater and surface water samples over the five rounds of sampling

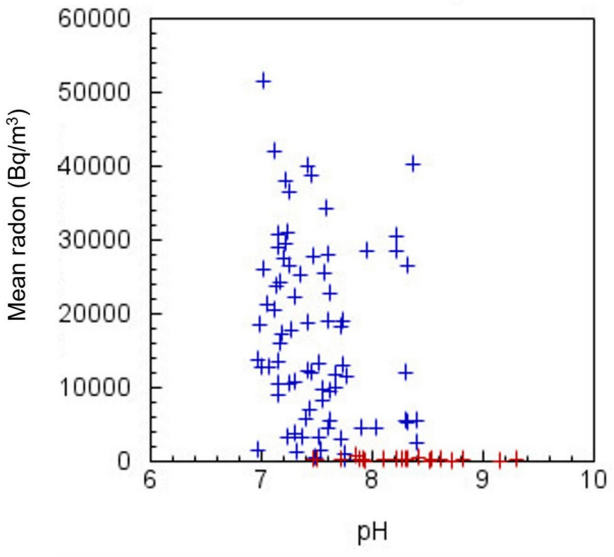

Fig. 15 Mean radon concentration vs. pH for the five rounds of sampling

Welverdiend B, and Hluvukani were much higher than those from other sample locations (Fig. 3), likely due to these areas being more populated compared to other locations in nature preserves with significantly less development. These three sample locations can therefore be considered as a separate group. Table 1 shows the average NO_3^- concentrations for groundwater and surface water samples across the five sampling rounds, as well as the overall averages. There are three averages given for the groundwater samples: one for all the samples, one without Welverdiend A, Welverdiend B and Hluvukani and one for just Welverdiend A, Welverdiend B, and Hluvukani.

The average surface water NO_3^- concentration remained relatively constant throughout the five rounds of sampling, excluding Round 1 where there was only one dam sampled. The groundwater NO_3^- concentrations (without Welverdiend A, Welverdiend B and Hluvukani) fluctuated without a clear pattern (Fig. 17). This trend does, however, not appear to be seasonal or related to rainfall events. The samples from Welverdiend A, Welverdiend B, and Hluvukani show an overall drastic increase in nitrate concentrations as sampling continued. According to Tredoux et al. (2009), on-site sanitation is the main source of nitrate pollution in southern Africa. When sampling in the communities of Welverdiend A and B it was noted that the boreholes were located downslope from the settlements, pit latrines, cattle kraals (enclosures) and livestock dipping tanks (where insecticides are used to control parasites), suggesting these are the likely sources of nitrate pollution.

The results indicate that groundwater generally exhibits higher total dissolved solids (TDS) and NO_3^- concentrations compared to surface water. This is particularly pronounced in more densely populated areas, such as Welverdiend and

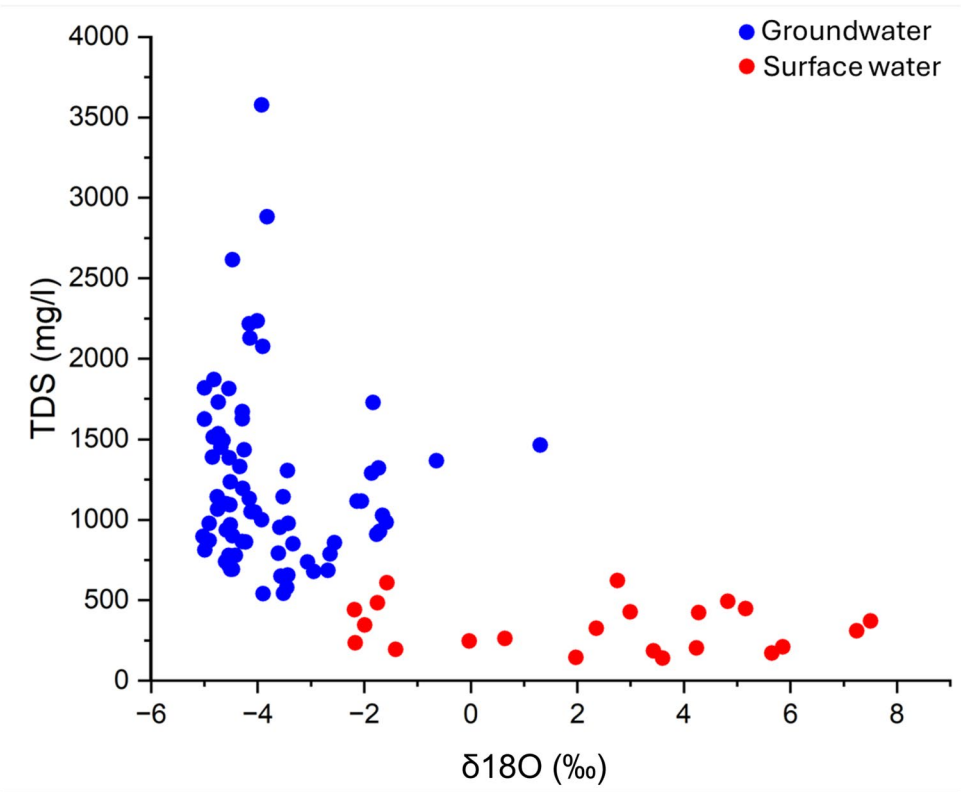

Fig. 16 Comparison of $\delta^{18}O$ and TDS concentrations in groundwater and surface water samples

Table 1 Average NO_3^- concentrations for surface water and groundwater samples, as well as the average groundwater concentration with the outliers removed

Round of sampling	Average NO_3^- (mg/l)			
	Surface water	Groundwater: All	Groundwater: Without Welverdiend A, Welverdiend B and Hluvukani	Groundwater: Just Welverdiend A, Welverdiend B and Hluvukani
September and October 2021	1.49	38.5	12.3	169.4
February 2022	6.30	71.8	18.2	339.6
May and June 2022	5.63	51.3	14.0	331.3
August and September 2022	5.76	81.8	18.3	526.1
November 2022	5.76	148	12.9	1092
All Rounds	5.56	83.1	15.6	508.7

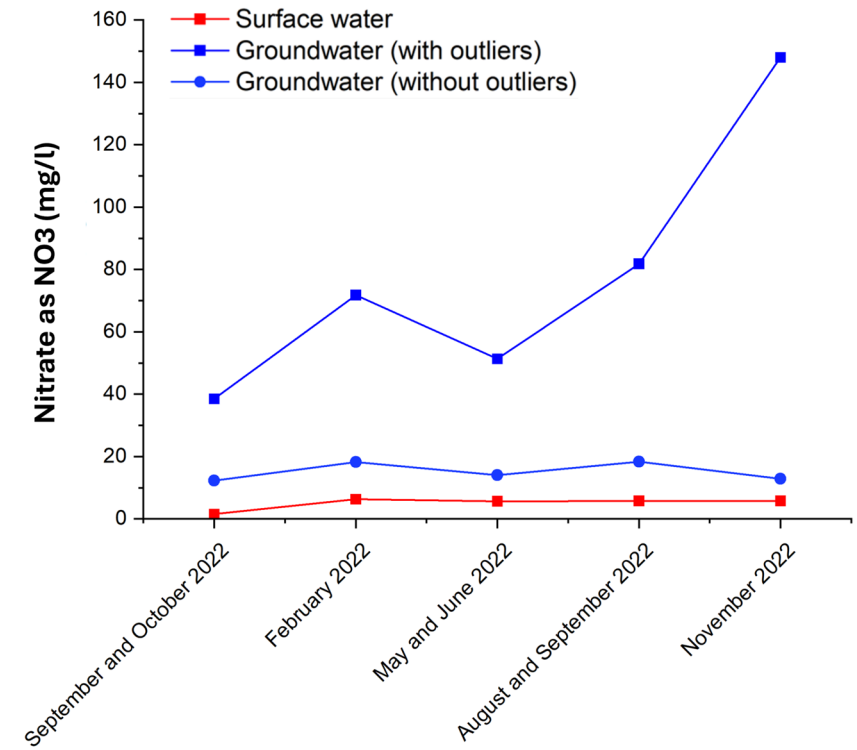

Fig. 17 Average nitrate concentrations for surface water and groundwater samples, including the groundwater averages with outliers removed

Hluvukani, where NO_3^- levels exceed safe drinking water guidelines. These findings align with prior studies in southern Africa (Tredoux et al. 2009; Baloyi and Diamond 2019; Masindi and Foteinis 2021) that identify on-site sanitation systems and agricultural activities as significant contributors to groundwater contamination. The proximity of boreholes to pit latrines, cattle kraals, and agricultural fields likely facilitates nitrate leaching into the groundwater.

The weighted regression equation for the local meteoric water line is $\delta D = 6.2\delta^{18}O + 8.3$, having a shallower gradient than the GMWL. A weighted meteoric water regression line was used as it better characterizes the average rainfall for the area because it considers heavier rainfall events and minimizes the effect of evaporation from smaller rainfall events (Hughes and Crawford 2012). The shallower gradient of the LMWL compared with the GMWL is common in warmer regions (Clark 2015). Looking at Fig. 13, it can be seen that the months with the lowest rainfall (February, September and October) had the heaviest isotopic compositions. This is part of the "amount effect", where there is a shift towards lighter isotope compositions with heavier rainfall events and vice versa (Diamond 2022). A possible reason for

the high δD values for September is that this month marked the first rainfall event after the dry winter season ended, and humidity was therefore very low. Raindrops are subject to evaporation during precipitation, and as evaporation is relatively high in dry air, the lighter isotopes would have been preferentially evaporated.

As seen in Fig. 12, the groundwater samples have a lighter isotopic composition than the surface water samples. Petersen et al (2023), who used stable isotopes to identify surface water–groundwater interactions in the Kruger National Park, also found that their groundwater samples had more negative isotopic ratios compared to the rain and surface water samples. The light isotope composition is likely due to recharge occurring as a result of heavy rainfall events when the lighter isotopes condense and precipitate. The groundwater samples plot along the lower end of the surface water samples local evaporation line (LEL, $\delta D = 5.1 \times \delta^{18}O + 0.3$) and to the right of the lower end of the LMWL. The regression line calculated for the groundwater samples had the equation $\delta D = 4.9 \times \delta^{18}O – 1.7$. The equation has a gradient very close to the LEL but with a lower intercept, suggesting that some evaporation is taking place before the rainwater enters the aquifer or there is mixing of less evaporated groundwater with infiltration of evaporated surface water. Groundwater samples varied by 22.7 ‰ for δD and 2.1 ‰ for $\delta^{18}O$, however, when focusing on the averages for each round of sampling in Fig. 14, the groundwater isotope compositions were found to remain relatively constant over the sampling period. During September/October 2021, the groundwater sample from Kokomoya had an isotopic composition that plotted closer to the surface water samples rather than the other groundwater samples. This could be from insufficient purging of the borehole prior to sampling, which could have resulted in the collection of wellbore water rather than fresh groundwater. The heavy isotope compositions of the surface water samples are likely a sign of enrichment due to evaporation. In February 2022, SANSW, THORSW1, and THORSW2, and in May/June 2022, THORSW2 had isotope compositions that overlapped with the groundwater samples, perhaps indicating some groundwater–surface water interaction.

During the final round of sampling, only the large dams at Manyeleti, Andover, and Sandringham had water in them; the rest of the sampling sites had dried up. Manyeleti and Andover were the most enriched in heavier isotopes during the final round of sampling in November 2022, likely due to these dams having the largest surface areas and therefore subject to greater evaporation. The dam at Sandringham also had more vegetation, specifically water lilies, that covered a large portion of the surface area of the dam, somewhat reducing the amount of evaporation.

The isotopic data (δD and $\delta^{18}O$) demonstrate distinct differences between groundwater and surface water, with groundwater exhibiting lighter isotopic compositions. This suggests that groundwater recharge is predominantly driven by heavy rainfall events, which are less influenced by evaporation. The surface water, on the other hand, shows evidence of evaporation, particularly in large dams like Manyeleti and Andover, which is reflected in their heavier isotopic signatures.

The distinct separation between stable isotope compositions of surface and groundwater suggest limited groundwater–surface water interaction. The drying up of all streams by the end of the dry season proves that the water table is too low to provide perennial baseflow. This may be a natural feature of this region, or may be due to the usage of groundwater by humans. An audit of groundwater use and a water budget for the region may help to reveal if groundwater usage is having a negative impact on streamflow.

Uranium concentrations in the groundwater samples were below the detection limit of 0.015 mg/l for the analysis performed by Aquatico. It was therefore not possible to see if there was a relationship between radon and uranium concentrations. There were also no clear relationships between pH, DO, EC, TDS, SAL, ORP, and radon concentrations. This lack of a clear correlation between radon levels and geological formations aligns with previous studies such as Cho and Choo (2019) who observed similar independence of radon from common geochemical parameters, suggesting that radon migration may be controlled more by local hydrodynamic conditions rather than rock type alone. The high radon concentrations observed in this study's groundwater samples are consistent with those found in South Africa's Table Mountain Group aquifer system and in Ethiopia's Upper Awash Basin, where radon levels are elevated in fractured, uranium-rich formations (Strydom et al. 2021 and Tadesse et al. 2023). These structural features seem to play a critical role in allowing for the movement of radon through faults and fractures, leading to variations in concentrations across different geological formations.

THORSW2 was the only surface water sample to have a radon concentration as high as some groundwater samples during the May/June 2022 round of sampling. ANDSW, WelASW, SANSW, and THORSW1 were the only surface water samples that contained radon during all the rounds that they were sampled. However, during August/September 2022 all the surface water samples contained radon. The radon in the surface water, along with the pH, TDS, ORP and DO values that overlapped with the groundwater samples, could be a sign of groundwater discharge into the river and dams. This aligns with the findings from South Korea, where radon concentrations in groundwater systems were affected by seasonal shifts in river flow and dam discharge (Kim et al. 2020). These seasonal variations suggest that radon concentrations in

surface water could be used as indicators of periods of enhanced groundwater discharge.

The Piper plot and Stiff diagrams further suggest that water chemistry is heavily influenced by the underlying geology, with the Klaserie and Makhutswi gneisses producing distinct chemical signatures. Samples from the Timbavati Gabbro, particularly at UPCell, show elevated magnesium concentrations, consistent with weathering of mafic minerals such as olivine and pyroxene.

These findings highlight the complexity of groundwater–surface water interactions in the region and underscore the need for integrated water management strategies that consider both natural geological processes and human impacts.

Conclusions

This study has significantly enhanced the understanding of the hydrochemistry in the Greater Timbavati area, revealing distinct differences between groundwater and surface water. Groundwater exhibited higher TDS values, primarily due to the effects of weathering and water–rock interactions, while surface water showed signs of evaporation. The groundwater samples were further divided into three distinct chemical groups, each correlating with the underlying geology. Nitrate contamination was particularly high in groundwater from populated areas, likely stemming from human, animal, and agricultural waste. This finding underscores the urgent need for improved sanitation infrastructure to reduce contamination risks. Isotopic analysis indicated that groundwater recharge is influenced by heavy rainfall, with some evaporation occurring prior to recharge. The detection of radon in both groundwater and surface water also suggests potential groundwater discharge into surface water bodies. The strong distinction between groundwater and surface water hydrochemistry, stable isotopes, and radon values, as well as the drying up of streams by the end of the dry season, suggests low water tables and limited groundwater–surface water interaction. An audit into groundwater usage in the region may help determine if this is natural or caused by overabstraction.

To safeguard water quality, water managers should prioritize addressing nitrate contamination by improving sanitation systems, such as lining pit latrines and controlling agricultural runoff. The isotopic data and radon measurements can also be used to monitor groundwater recharge and manage water abstraction sustainably, ensuring long-term water security in this semi-arid region. Future research should focus on nitrogen isotope analysis to better identify contamination sources and continued monitoring of radon levels to further understand groundwater–surface water interactions. Overall, this baseline assessment provides essential data for policymakers and conservationists, supporting informed water management and sustainability efforts in the Greater Timbavati area.

Acknowledgements This endeavor would not have been possible without the financial support of the Water Research Commission and the National Nuclear Regulator. Sincere thanks to Acorns to Oaks, Andover Nature Reserve, Baobab, Meyer de Kock and the Hans Hoheisen Wildlife Research Station, Hluvukani Animal Clinic, Honeyguide, Kruger to Canyons, Manyeleti Game Reserve, Mpumalanga Tourism and Parks Agency, Nourish Eco Village, Sandringham Private Nature Reserve, Sigagula Children's Centre, South African Wildlife Collage, Thorneybush Private Game Reserve, Wits Rural Campus and the community leaders of Welverdiend for allowing sampling on their land.

Author Contribution The study was conceptualized and conducted by Kirsten Raible as part of her MSc research. Material preparation, data collection, analysis, and the first draft of the manuscript were completed by Kirsten Raible. Dr Roger Diamond and Prof Matthys Dippenaar provided supervision, critical feedback, and editorial input throughout the writing process. All authors read and approved the final manuscript.

Funding Open access funding provided by University of Pretoria. This work was supported by the Water Research Commission and the National Nuclear Regulator (CNSS0117-A5-UP).

Data Availability The datasets generated and analyzed during the study consist of field notes and laboratory results. This data is not publicly available but is available from the corresponding author on reasonable request.

Declarations

Ethics approval and consent to participate Not applicable.

Consent for publication Not applicable.

Competing interests The authors have no relevant financial or non-financial interests to disclose.

Conflict of interest The authors declare that they have no conflict of interest.

References

Abiye TA, Demlie MB, Mengistu H (2021) An overview of aquifer physiognomies and the δ18O and δ2H distribution in the South

African groundwaters. Hydrology 8:68. https://doi.org/10.3390/hydrology8020068
Alabdula'aly AI (2014) Occurrence of radon in groundwater of Saudi Arabia. J Environ Radioact 138:186–191
Allsopp HL, Kramers JD, Jones DL, Erlank AJ (1989) The age of the Umkondo Group, eastern Zimbabwe, and implications for palaeomagnetic correlations. S Afr J Geol 92:11–19
Anhaeusser CR, Johnson MR, Thomas RJ (2006) Ultramafic and mafic intrusions of the Kaapvaal Craton. In: The geology of South Africa. Geological Society of South Africa, Johannesburg/Council for Geoscience, Pretoria, pp 95–134
Appelo CAJ, Postma D (2005) Geochemistry, groundwater and pollution, 2nd edn. CRC Press, Amsterdam Baskaran M (2016) Radon: A tracer for geological, geophysical and geochemical studies. Springer, https://doi.org/10.1007/978-3-319-21329-3
Baloyi RS, Diamond RE (2019) Variable water quality of domestic wells emphasizes the need for groundwater quality monitoring and protection: Stinkwater, Hammanskraal, Gauteng. Water SA 45:216–224. https://doi.org/10.4314/wsa.v45i2.08
Barton JM Jr (1984) Timing of ore emplacement and deformation, Murchison and Sutherland greenstone belts, Kaapvaal craton. In: Gold'82: the geology, geochemistry and genesis of gold deposits. Symposium, pp 629–644
Baskaran M (2016) Radon: a tracer for geological, geophysical and geochemical studies. Springer. https://doi.org/10.1007/978-3-319-21329-3
Brandl G (1985) 1:25000 Geological Series map (2330 Tzaneen). Geological Survey of South Africa
Brandl G, Kröner A (1993) Preliminary results of single zircon studies from various Archaean rocks of the Northeastern Transvaal. In: International colloquium on Africa geology, pp 54–56
Cho BW, Choo CO (2019) Geochemical behaviour of uranium and radon in groundwater of Jurassic granite area, Icheon, Middle Korea. Water (Basel) 11:1278
Cho B-W, Choo CO, Kim MS, Hwang J, Yun U, Lee S (2015) Spatial relationships between radon and topographical, geological, and geochemical factors and their relevance in all of South Korea. Environ Earth Sci 74:5155–5168
Clark I (2015) Groundwater Geochemistry and Isotopes, 1st edn. CRC Press, Boca Raton
Clubley-Armstrong AR (1979) The geology of the southern Kruger National Park, from west of Pretoriuskop eastward to the Lebombo Mountains and the Mocambique border. Geological Survey of South Africa (Unpublished)
Council for Geoscience (n.d.) 1:1 000 000 geological map of South Africa – geological polygons [vector layer, CGS_RSA1M_geological_polygons]. Council for Geoscience, Pretoria
Craig H (1961) Isotopic variations in meteoric waters. Science (1979) 133:1702–1703
Department of Water Affairs and Forestry (2004) Olifants Water Management Area: Internal Strategic Perspective. Prepared by GMKS, Tlou and Matji and WMB on behalf of the Directorate: National Water Resource Planning. DWAF Report No P WMA 04/000/00/0304. South Africa
Department of Water and Sanitation (DWS) (2017) Water Management System GIS Data – Quaternary Catchments. Available at: https://www.dws.gov.za/iwqs/wms/data/000key2data.asp [Accessed 14 June 2022].
Diamond RE, Harris C (2019) Stable isotope constraints on hydrostratigraphy and aquifer connectivity in the Table Mountain Group. S Afr J Geol 122:317–330. https://doi.org/10.25131/sajg.122.0021
Diamond E (2022) Stable Isotope Hydrology, 1st edn. The Groundwater Project, Ontario. https://doi.org/10.21083/978-1-77470-043-3
Ding Z, Ma J, Zhao W et al (2013) Profiles of geochemical and isotopic signatures from the Helan Mountains to the eastern Tengger Desert, northwestern China. J Arid Environ 90:77–87. https://doi.org/10.1016/j.jaridenv.2012.10.01
Dube T, Shoko C, Sibanda M, Baloyi MM, Molekoa M, Nkuna D, Rafapa B, Rampheri BM (2020) Spatial modelling of groundwater quality across a land use and land cover gradient in Limpopo Province, South Africa. Phys Chem Earth Parts A/B/C 115:102820
Esri (2023) South Africa country boundaries 2023 [GIS dataset]. Esri Aid & Development Team. Data sourced from Michael Bauer Research GmbH and Statistics South Africa. ArcGIS Online
Gordon-Welsh JF (1980) A gravity and magnetic profile northeast of Orpen in the Kruger National Park. In: Internal report of the geological survey of southern Africa (Unpublished)
Graham JP, Polizzotto ML (2013) Pit latrines and their impacts on groundwater quality: a systematic review. Environ Health Perspect 121:521–530. https://doi.org/10.1289/ehp.1206028
Grolander S (2009) Radon as a groundwater tracer in Forsmark and Laxemar. (SKB-R--09–47). Sweden
Hanson RE, Gose WA, Crowley JL, Ramezani J, Bowring SA, Bullen DS, Hall RP, Pancake JA, Mukwakwami J (2004) Paleoproterozoic intraplate magmatism and basin development on the Kaapvaal Craton: age, paleomagnetism and geochemistry of ~1.93 to ~1.87 Ga post-Waterberg dolerites. S Afr J Geol 107:233–254. https://doi.org/10.2113/107.1-2.233
Hao S, Li F, Li Y, Gu C, Zhang Q, Qiao Y, Jiao L, Zhu N (2019) Stable isotope evidence for identifying the recharge mechanisms of precipitation, surface water, and groundwater in the Ebinur Lake basin. Sci Total Environ 657:1041–1050. https://doi.org/10.1016/j.scitotenv.2018.12.102
Harkness JS, Swana K, Eymold WK, Miller J, Murray R, Talma S, Whyte CJ, Moore MT, Maletic EL, Vengosh A (2018) Pre-drill groundwater geochemistry in the Karoo Basin, South Africa. Ground Water 56:187–203. https://doi.org/10.1111/gwat.12635
Hughes CE, Crawford J (2012) A new precipitation weighted method for determining the meteoric water line for hydrological applications demonstrated using Australian and global GNIP data. J Hydrol (Amst) 464:344–351. https://doi.org/10.1016/j.jhydrol.2012.07.029
Kim J, Kim H, Lee KK (2020) Application of 222Rn and microbial diversity to characterize groundwater/surface–water interactions in a riverside area (South Korea). Hydrogeol J 28(4):1173–1189. https://doi.org/10.1007/s10040-020-02148-4
Knutsson G, Olofsson BO (2002) Radon content in groundwater from drilled wells in the Stockholm region of Sweden
Lachassagne P, Dewandel B, Wyns R (2021) Hydrogeology of weathered crystalline/hard-rock aquifers—guidelines for the operational survey and management of their groundwater resources. Hydrogeol J 29:2561–2594. https://doi.org/10.1007/s10040-021-02339-7
Litt BR, Korn LR, Moser FC, Bell C, Clare AK, Uptegrove J, Key RM (1992) Influence of geology on radon in groundwater supplies of the New Jersey Highlands. Department of Environmental Protection and Energy, Division of Science and Research
Liu Y, Yamanaka T (2012) Tracing groundwater recharge sources in a mountain–plain transitional area using stable isotopes and hydrochemistry. J Hydrol (Amst) 464:116–126. https://doi.org/10.1016/j.jhydrol.2012.06.053
Masindi V, Foteinis S (2021) Groundwater contamination in sub-Saharan Africa: implications for groundwater protection in developing countries. Cleaner Engineering and Technology 2:100038
McGill BM, Altchenko Y, Hamilton SK, Kenabatho PK, Sylvester SR, Villholth KG (2019) Complex interactions between climate change, sanitation, and groundwater quality: a case study from Ramotswa, Botswana. Hydrogeol J 27:997–1015. https://doi.org/10.1007/s10040-018-1901-4

Peng T-R, Huang C-C, Zhan W-J, Wang C-H (2016) Assessing groundwater sources and their association with reservoir water using stable hydrogen and oxygen isotopes: a case study of the Taipei Basin, northern Taiwan. Environ Earth Sci 75:1–13. https://doi.org/10.3390/geosciences8030084

Petersen RM, Nel JM, Strydom T, Riddell E, Coetsee C, February E (2023) The use of stable isotopes to identify surface water–groundwater interaction in the Kruger National Park, South Africa. Water SA, 49(2), 96–102. https://doi.org/10.17159/wsa/2023.v49.i2.3992

Phungela TT, Maphanga T, Chidi BS, Madonsela BS, Shale K (2022) The impact of wastewater treatment effluent on Crocodile River quality in Ehlanzeni District, Mpumalanga Province, South Africa. S Afr J Sci 118:1–8

Poujol M, Robb LJ, Respaut J-P, Anhaeusser CR (1996) 3.07-2.97 Ga greenstone belt formation in the northeastern Kaapvaal Craton; implications for the origin of the Witwatersrand Basin. Econ Geol 91:1455–1461

Putman AL, Fiorella RP, Bowen GJ, Cai Z (2019) A global perspective on local meteoric water lines: meta-analytic insight into fundamental controls and practical constraints. Water Resour Res 55:6896–6910. https://doi.org/10.1029/2019WR025181

Robb LJ, Brandl G, Anhaeusser CR, Poujol M, Johnson MR, Thomas RJ (2006) Archaean granitoid intrusions. Geol S Afr 57–94

Saggerson EP, Logan CT (1970) Distribution controls of layered and differentiated mafic intrusions in the Lebombo volcanic sub-province. Spec Publ Geol Soc S Afr 1:721–733

Schutte IC (1986) The general geology of the Kruger National Park. Koedoe 29:13–37

Strydom T, Nel JM, Nel M, Petersen RM, Ramjukadh CL (2021) The use of radon (Rn222) isotopes to detect groundwater discharge in streams draining Table Mountain Group (TMG) aquifers. Water SA 47(2):194–199. https://doi.org/10.17159/wsa/2021.v47.i2.10915

Tadesse E, Azagegn T, Alemayehu T (2023) Characterizing groundwater and surface water interaction using geological, environmental tracers (222Rn, EC, δ18O, and δ2H) and baseflow index methods for part of the Upper Awash and the adjacent Blue Nile Basin, Ethiopia. J Afr Earth Sci. https://doi.org/10.1016/j.jafrearsci.2023.104992

Tommasino L (2005) Radon. J Chem Educ 82:32–44

Tredoux G, Engelbrecht P, Israel S (2009) Nitrate in Groundwater: Why is it a hazard and how to control it? WRC Report No. TT 410/09, Water Research Commission, Stellenbosch

Venter FJ, Gertenbach WPD (1986) A cursory review of the climate and vegetation of the Kruger National Park. Koedoe 29(1):139–148

Walraven F (1986) The Timbavati Gabbro of the Kruger National Park. Koedoe 29:69–84

Walraven F, Hartzer FJ (1986) Sheet 2530 Barberton (1: 250 000 Geological Series). Geol Surv S Afr

Walraven F (1989) The geology of the Pilgrim's Rest area. https://api.semanticscholar.org/CorpusID:127896541

West AG, February EC, Bowen GJ (2014) Spatial analysis of hydrogen and oxygen stable isotopes ("isoscapes") in ground water and tap water across South Africa. J Geochem Explor 145:213–222. https://doi.org/10.1016/j.gexplo.2014.06.009

Wright EP (1992) The hydrogeology of crystalline basement aquifers in Africa. Geological Society, London, Special Publications 66:1–27. https://doi.org/10.1144/GSL.SP.1992.066.01.01

Yeh H-F, Lee J-W (2018) Stable hydrogen and oxygen isotopes for groundwater sources of Penghu Islands, Taiwan. Geosciences 8:84. https://doi.org/10.3390/geosciences8030084

Yeh H-F, Lee C-H, Hsu K-C (2011) Oxygen and hydrogen isotopes for the characteristics of groundwater recharge: a case study from the Chih-Pen Creek basin, Taiwan. Environ Earth Sci 62:393–402. https://doi.org/10.1007/s12665-010-0534-2

Zhu S, Zhang F, Zhang Z et al (2019) Hydrogen and oxygen isotope composition and water quality evaluation for different water bodies in the Ebinur Lake watershed, northwestern China. Water 11:1–35. https://doi.org/10.3390/w11102067